International Journal of Nanomedicine

Dovepress
open access to scientific and medical research

Open Access Full Text Article

ORIGINAL RESEARCH

Effects of PEGylation on capture of dextran-coated magnetic nanoparticles in microcirculation

This article was published in the following Dove Press journal:
International Journal of Nanomedicine

Chien-Yu Chiu[1,2]
Tze-Wen Chung[3,4]
Si-Yi Chen[2]
Yunn-Hwa Ma[2,5]

[1]Graduate Institute of Biomedical Sciences, College of Medicine, Chang Gung University, Guishan, Taoyuan City 33302, Taiwan, ROC; [2]Department of Physiology and Pharmacology, College of Medicine, Chang Gung University, Guishan, Taoyuan City 33302, Taiwan, ROC; [3]Department of Biomedical Engineering, National Yang-Ming University, Beitou, Taipei City 11221, Taiwan, ROC; [4]Center for Advanced Pharmaceutical Research and Drug Delivery, National Yang-Ming University, Beitou, Taipei City 11221, Taiwan, ROC; [5]Department of Neurology, Chang Gung Memorial Hospital, Guishan, Taoyuan City 33305, Taiwan, ROC

Background: Magnetic nanoparticles (MNPs) can be localized against hemodynamic forces in blood vessels with the application of an external magnetic field. In addition, PEGylation of nanoparticles may increase the half-life of nanocomposites in circulation. In this work, we examined the effect of PEGylation on the magnetic capture of MNPs in vivo.

Methods: Laser speckle contrast imaging and capillaroscopy were used to assess the magnetic capture of dextran-coated MNPs and red blood cell (RBC) flow in cremaster microvessels of anesthetized rats. Magnetic capture of MNPs in serum flow was visualized with an in vitro circulating system. The effect of PEGylation on MNP-endothelial cell interaction was studied in cultured cells using an iron assay.

Results: In microcirculation through cremaster muscle, magnet-induced retention of 250 nm MNPs was associated with a variable reduction in RBC flow, suggesting a dynamic coupling of hemodynamic and magnetic forces. After magnet removal, faster restoration of flow was observed in PEG(+) than PEG(–) group, which may be attributed to a reduced interaction with vascular endothelium. However, PEGylation appears to be required for magnetic capture of 50 nm MNPs in microvessels, which was associated with increased hydrodynamic diameter to 130±6 nm in serum, but independent of the ς-potential.

Conclusion: These results suggest that PEGylation may enhance magnetic capture of smaller MNPs and dispersion of larger MNPs after magnet removal, which may potentially affect the targeting, pharmacokinetics and therapeutic efficacy.

Keywords: polyethylene glycol, magnetic nanoparticles, hemodynamics, microcirculation, magnetic targeting

Background

Magnetic localization of nanoparticles with an iron oxide core is a promising approach for target drug delivery.[1–5] With the superparamagnetic characteristics of the nano-sized iron oxide core, magnetic nanoparticles (MNPs) can be manipulated with an external magnetic field and thereby serve as carriers for delivery of drugs.[1–4,6,7] To achieve local accumulation of MNPs, various magnetic field designs have been tested ex vivo[8] and in vivo,[9–23] including alternating current-induced magnetic field[9] and NdFeB magnet applied in a stationary[8,10–16,20–23] or mobile[17-19] manner. Magnetic force-induced local retention of MNPs with particle sizes in the range of 130–366 nm has been demonstrated with good reproducibility in vivo,[11,12,14,16,20–23] including in vessels of different sizes[11,12] and tumor tissues.[14,16,20–23] Magnetic targeting with these MNPs may serve as a feasible strategy for delivery of thrombolytic[17,19,24,25] and

Correspondence: Yunn-Hwa Ma
Department of Physiology and Pharmacology, Chang Gung University, 259 Wen-Hwa 1st Road, Guishan District, Taoyuan City 33302, Taiwan, ROC
Tel/Fax +886 3 211 8800 ext 5152 or 5266
Email yhma@mail.cgu.edu.tw

submit your manuscript | www.dovepress.com
DovePress
http://doi.org/10.2147/IJN.S204844

chemotherapeutic[13,14,16,22,23] drugs. The therapeutic efficacy will be determined by strategic coupling of targeting, which depends on the properties of the particles and applied field, and drug release at the site of action. In target thrombolysis, interaction of the magnetic nanocomposites with the fibrin clot in the rat embolic model requires application of a mobile rather than a stationary magnet.[17] In addition, magnetic force may be applied to control release of encapsulated drugs to ensure thrombolytic efficiency in vivo.[25]

Following in vivo administration, MNPs are taken up by the reticuloendothelial system (RES) within minutes.[3,6] The fate of MNPs subjected to phagocytosis by RES depends on the size, surface modification, chemical composition, surface charge and hydrophobicity of MNPs.[2,3,7,26–28] Specifically, surface modification or polymer coating was shown to improve stability, dispersity and biocompatibility of MNPs.[2,3,7,26–28] The polymer, polyethylene glycol (PEG), is a stable, biocompatible, hydrophilic polymer, which has been extensively studied for applications to drug or gene delivery.[29–31] Immobilized PEG on the nanoparticle alters the surface characteristics of the particle, which is dependent on the molecular weight and polymer conformation. PEG modification can also hinder interaction with plasma proteins and reduce plasma protein adsorption on the surface of the nanoparticles.[29,30,32] Moreover, PEG reduces the response of the immune system to nanoparticles.[3,29–31,33] This in turn reduces clearance of the nanoparticles from the circulation, and thereby allows a longer circulation time and more nanoparticle accumulation at the target site.[33–35] Nevertheless, PEGylation may also reduce internalization of MNPs by tumor cells[30,36–38] as well as endothelial cells[38,39] in culture, and thus potentially reduce intracellular delivery of drugs.

After intravascular administration, nanoparticles will initially contact the endothelium of the blood vessel, which is composed of a thin continuous layer of cell lining. The interaction of multifunctional nanoparticles with the endothelium is important,[38–42] as it is the main target in the treatment of disease, including inflammatory, cardiovascular and oncological diseases.[43,44] PEG coating reduces adhesion of polystyrene spheres to endothelial monolayer under physiological shear in vitro.[39] In addition, PEG modulates the intracellular behavior of nanoparticles, probably due to protein adsorption.[45] We recently demonstrated that PEGylation of dextran-coated MNPs may alter particle properties in circulation.[46] Although PEGylated nanocomposites with iron oxide core can be magnetically captured in vivo,[16,47] the effect of PEGylation on the behavior of MNPs subjected to magnetic capture in circulation has not been investigated.

In the current study, the effect of PEG modification on the behavior of dextran-coated MNP in response to magnetic and hemodynamic forces was assessed by visualization of red blood cell flow in microvessels in vivo, using a cremaster microcirculatory preparation of rats.[11] The results suggest that PEGylation may induce a shielding effect, facilitate capture and escape of MNPs in a size-dependent manner, and modulate blood flow in the presence of a magnetic field.

Methods

Materials

Dextran-coated magnetic nanoparticles (MNPs; 50 and 250 nm) with (nanomag®-D PEG-COOH) or without (nanomag®-D COOH) polyethylene glycol (PEG; 600 daltons) were purchased from Micromod Partikeltechnologie GmbH (Rostock, Germany). Neodymium (NdFeB) magnets were purchased from New Favor Industry Co., Ltd (Taiwan). Hydroxyethyl starch solution (6%, Voluven®) was purchased from Fresenius Kabi (Germany). Heparin (50,000 units), Inactin® (sodium salt of ethyl-[1-methyl-propyl]-malonyl-thio-urea), fetal bovine serum (FBS), ammonium persulfate and potassium thiocyanate (KSCN) were purchased from Sigma (St Louis, MO, USA). M199 medium and trypsin-ethylenediaminetetra acetic acid were purchased from Gibco BRL (Grand Island, NY, USA). Horse serum was purchased from Hyclone® (Logan, UT, USA). Penicillin/streptomycin/amphotericin and endothelial cell growth supplement (ECGS) were purchased from Upstate Biotechnology (Lake Placid, NY, USA).

Size and ζ-potential measurement of nanoparticles

The hydrodynamic size distribution and the ζ-potential of MNPs were determined by dynamic light scattering and electrophoretic light scattering, respectively, using a particle analyzer (NanoPlus, Micromeritics; GA, USA). MNPs were suspended at a concentration of 0.05 mg/mL in deionized water (DIW), phosphate buffered saline (PBS; NaCl 137 mM, KCl 2.7 mM, Na_2HPO_4 10 mM, KH_2PO_4 2 mM; pH 7.4) or particle-free horse serum, which was subjected to a series of centrifugation to ensure removal of suspended particles. Briefly, the horse serum was centrifuged at 300×g for 15 mins (Sorvall RT6000B;

MA, USA); the supernatant was then centrifuged at 3,800×g for 10 mins (Beckman coulter AV anti J-E centrifuge; CA, USA), followed by 100,000×g for 1 hr (Beckman coulter optima L-100 K; CA, USA) to remove any particular matter. After centrifugation and removal of the upper lipid layer, particle-free serum was obtained and used to mimick serum components in circulation. MNPs were suspended by a 10-mins sonication prior to the measurement at 25°C. PBS and serum samples were analyzed with identical parameter setting.

Cremaster muscle preparation

The cremaster muscle was prepared based on a previous study with minor modification,[11] and the experimental protocol was approved by the Institutional Animal Care and Use Committee at Chang Gung University, which is certified by the American Association for Accreditation of Laboratory Animal Care. Briefly, Sprague Dawley rats (330±7 g, n=23) were anesthetized using Inactin® (100 mg/kg; i.p.). After hair removal from the lower abdomen and the scrotum, a rectal probe was inserted to ensure the core body temperature at 37±1°C, followed by urinary bladder cannulation. The left cremaster muscle was dissected, and the testis was removed. From the left femoral artery, the iliac artery was cannulated in a retrograde manner with a PE50 tubing without interrupting the blood flow to the pudic epigastric artery, a branch of the iliac artery that supplies blood to the cremaster bed. Two small branches of the left iliac artery and pudic epigastric artery were ligated, allowing most of injected particles to reach the cremaster vasculature. With the cremaster vasculature remaining part of the rat circulation (Figure S1), the muscle was then placed in situ on a cylindrical NdFeB magnet (1.9 cm in diameter; 0.8 cm in thickness), and tension was applied. Saline-hydroxyethyl starch (1:2) mixture was continuously infused at a rate of 30 μL/min for injection of MNPs via an injection port on the intra-arterial catheter tubing. At completion of the study (see below), the rats were euthanized by cervical dislocation under anesthesia.

Laser speckle imaging

The laser speckle contrast imaging (MoorFLPI-2™; Moor Instruments, England) was used to monitor tissue blood flow changes in real time. A random speckled pattern is generated as blood cells move in the tissue, which is illuminated by a focused diode laser at 650 nm. The region of interest (ROIs) in the field of monitoring was analyzed with time. Blood flow is presented as 2-D images or tracings that were updated every 10 sec. The simultaneous recordings of flux and photo images reveal patterns of flow and MNP retention in a single microvessel. There are two major branches of microvessels in the cremaster muscles. For data analysis, six to eight ROIs in each branch were averaged to obtain perfusion values of each branch. The lowest blood flow occurred 4–13 mins after intra-arterial injection of MNPs (+MNP), and the flow 5 and 15 mins after removal of the magnet (-Mag) was calculated as percent basal level.

Capillaroscopy

Visualization and characterization of MNP capture in cremaster microcirculation were performed using the CapiScope Handheld Video Capillaroscope System (KK Technology, Honiton, England), which generated oblique profiled epi-illumination imaging by light-emitting diodes at a wavelength of 525~535 nm. In the image, RBCs were viewed as flowing subjects over a gray background, which delineates vessel wall as a faint contour, whereas MNP pellet captured by the magnet was observed as a dark subject. A color mode was used to increase the contrast for observation of the vessel wall. RBC flow and diameter of a single vessel was determined from the images.

In vitro circulation system

To observe magnetic capture of MNPs in a circulatory system, magnet-induced MNP retention in a silicon tubing (i.d. 2 mm; o.d. 4 mm) was recorded using a CCD camera (MD130, Sage Vision, Taiwan) controlled by Future WinJoe software (Future Optics, Hangzhou, China) mounted on a dissecting microscope (SL-620, Sage Vision, Taiwan). A permanent magnet (2×1×0.5 cm; 1.55 kG) was placed by the silicon tube at a 45° angle, 5 cm downstream from the injection site as illustrated in Figure 4A. The peristaltic pump (Masterflex® 7553–80, Vernon Hills, Il, USA) with silicone tubing (Peroxide; L/STM13 #96400-13 with i.d. 0.8 mm) induced a flow of 2 mL/min through the total length of 150 cm tubing filled with horse serum or hydroxyethyl starch solution. The horse serum was centrifuged at 100,000 g for 1 hr to remove particular matter prior to use. The shear stress of the system with serum was calculated to be 0.7 dyn/cm^2, using a viscosity of 1.66 mPa s.[48] In experiments with serum, particles (0.1 mg) were injected into the silicon tube in approximately 10 s, followed by a 10 mins observation period. In experiments with hydroxyethyl starch solution, particles (0.1 mg) and citrated whole blood (20 μL) were injected simultaneously, followed by a 1 min observation period. The

2-dimentional area of the particle retention in the silicon tube was analyzed by image-J software.

Endothelial cell culture

Human umbilical vein endothelial cells (HUVECs) were obtained with a protocol approved by the institutional review board of Chang Gung Memorial Hospital to study MNP-HUVEC interaction, as described previously.[38,40] HUVEC were cultured in M199 medium with FBS (10%), heparin (100 μg/mL), endothelial cell growth supplement (ECGS) (30 μg/mL) and penicillin/streptomycin/amphotericin (1%) at pH 7.4. The cells were maintained at 37°C in an incubator supplied with 5% CO_2 and used between passages 3–9.

Cellular uptake of MNPs

HUVECs were cultured in a 24-well culture plate with M199 medium to 90% confluence prior exposure to MNPs (100 μg/mL) with or without placement of the NdFeB magnet underneath the well for 0.5–6 hrs. All groups were subjected to the NdFeB magnet for 5 mins immediately after addition of MNPs to ensure sedimentation of the particles. After trypsinization, hydrochloric acid (10% v/v) was added to the cell pellet and incubated at 55°C for 4 hrs, followed by treatment with ammonium persulfate (1 mg/mL) and KSCN (1 M). The amount of cell-associated iron was determined by measurement of OD_{490} with a VICTOR3 Multilabel Plate Reader (PerkinElmer, Shelton, CT, USA). A standard curve with a known concentration of MNPs was prepared under identical conditions for the calibration.

Statistical analysis

Data are presented as mean ± SEM. All results were analyzed using a student's *t*-test, paired *t*-test or one-way analysis (ANOVA) with repeated time measurement followed by Duncan's post hoc test. Statistical significance was determined at $P<0.05$.

Results

Figure 1 illustrates hydrodynamic diameters and the ζ-potential of PEG(–) *vs* PEG(+) MNPs in PBS or serum. In PBS (Figure 1A), PEGylation induced no effect on ζ-potential or hydrodynamic size in either size of MNPs studied. In serum (Figure 1B), the hydrodynamic diameter of both the PEG(–) and PEG(+) MNPs of 250 nm increased to about 600 nm. However, only the hydrodynamic diameter of PEG(+) 50 nm MNPs increased in size with the corresponding PEG(–) MNPs remaining largely unchanged. Despite the very different sizes, the ζ-potentials of all MNPs in serum were similar and averaged from −7.2 to −8.2 mV, probably due to formation of protein corona.

Figure 2 illustrates images of MNP accumulation with time in a representative microvessel preparation of cremaster skeletal muscle with an underlying magnet. The upper panel shows the initial rapid flow through the vessel, and as early as 1 min after MNP (5 mg/kg) administration, the flow is reduced in a localized region. The corresponding lower panel provides photographs and the growing dark, localized region, reflecting the accumulation of MNPs. Such retention of MNPs interfered the speckle signals and left gray images at 2–10 mins after MNP administration. Gradual reduction of the RBC flow to 84% of basal level was measured upstream of the retention site 4 mins after administration of MNPs. Removal of the magnet 15 mins after administration resulted in the rapid removal of the MNPs and restoration of the flow. In contrast, the flow of the parallel vessel remained relatively stable at 93±2% (n=5) of the basal value at these time points studied.

Supplemental data (Figure S2) provide an expanded view of the accumulation site, where magnetic capture of MNPs occurred in the cremaster microvessels (photo views) and the flow was affected not only in the parent vessel but also in downstream branches as evident by the gray area in the flux view. However, no significant difference was observed comparing RBC flow up- vs downstream of the retention sites without any branch in between (A, B, F, G, H; n=5).

Figure 3 shows the results from injection of PEGylated MNPs subjected to magnetic capture on RBC flow in cremaster microvessels in vivo. After intra-arterial administration of 250 nm particles under magnetic capture (Figure 3A–C), RBC flow was reduced in most of the ROIs studied; however, in some vessels, the RBC flow fluctuated even with the magnet underneath the muscle piece. After magnet removal (-Mag), the flow was immediately restored in PEG(+) rat, whereas the flow in most vessels of the PEG(–) rat was at best only partially restored after magnet removal (Figure 3A). Most tracings, which represent the relative changes of RBC flow with time, of vessels in the PEG(+) rat recovered to near basal levels of individual vessel after magnet removal (Figure 3A). This was also observed in the representative flux images from the same rat in Figure 3B. MNPs of 250 nm with vs without PEG significantly reduced basal blood flow by 73% (n=11

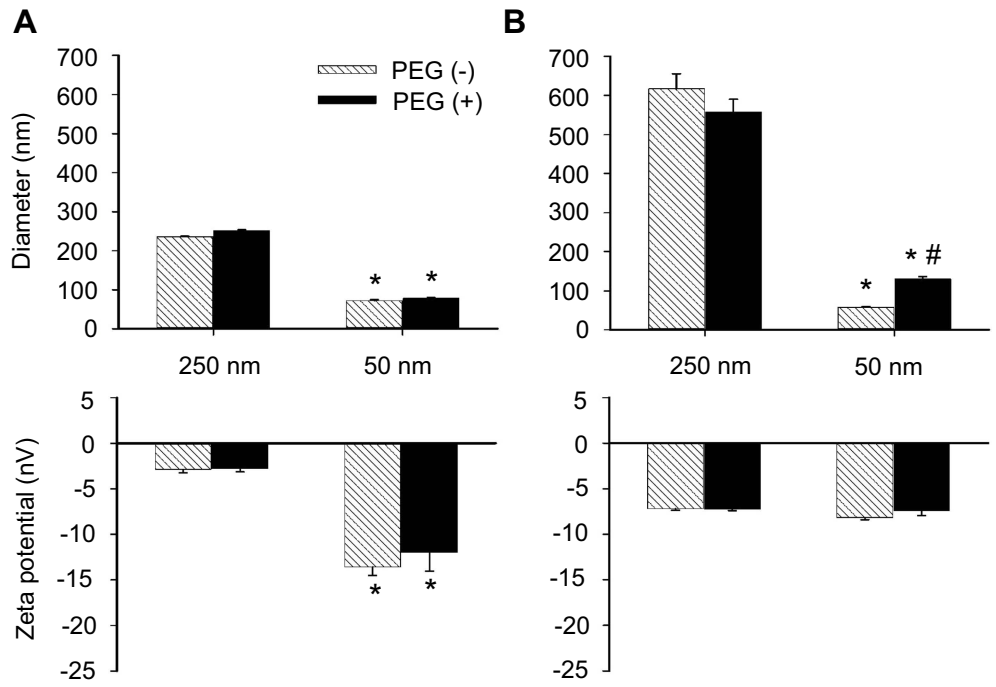

Figure 1 Diameter and ς-potential of MNPs with or without PEG. Particle size and ζ-potential of MNPs were measured in phosphate-buffered saline (PBS, **A**) or serum (**B**). The values shown are mean ± SE (n=3–4). $^{*\#}p<0.05$ compared with the corresponding 250 nm particles and PEG(–) groups, respectively.

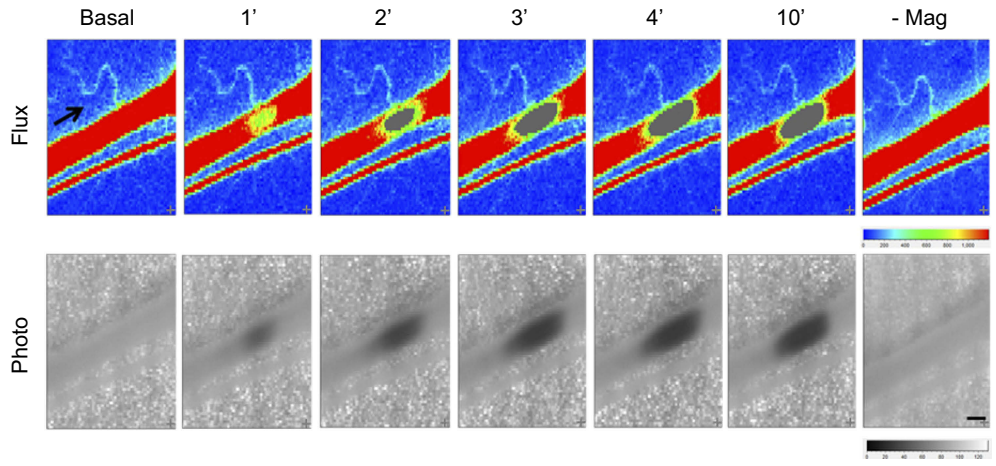

Figure 2 Magnetic capture of MNP and subsequent flow changes in microvessels. MNPs (5 mg/kg, 250 nm) were administered intra-arterially to the left cremaster muscle with an NdFeB magnet placed underneath. MNP accumulation 1 to 14 mins after administration is illustrated as flux and photo images. The arrow in the flux images indicates the flow direction of the adjacent vessel. Representative capture of MNP in a microvessel with time were observed, followed by removal of the magnet (-Mag) 14 mins after MNP administration. Scale bar indicates 0.3 μm.

branches from 5 rats) vs 58% (n=9 branches from 5 rats), respectively (Figure 3C); however, no significant effect was observed between the PEG(+) and PEG(–) groups. Five minutes after magnet removal (-Mag), significant restoration of the flow was observed in both PEG(+) vs PEG(–) groups. Fifteen minutes after magnet removal, the flow of the PEG(+) group returned to near the basal level, which is significantly higher than that in the PEG(–) group ($P<0.05$).

In another group of rats receiving 50 nm MNPs, distinct tissue perfusion patterns were observed. Magnetic capture-induced flow reduction occurred only in the rat receiving PEG(+), but not PEG(–) MNPs (Figure 3D and E). The magnetic capture of PEGylated MNPs reduced flow in almost all vessels studied in this representative rat, demonstrating a dynamic retention pattern with the magnet in place; whereas magnet removal partially restored the flow (Figure 3D and E).

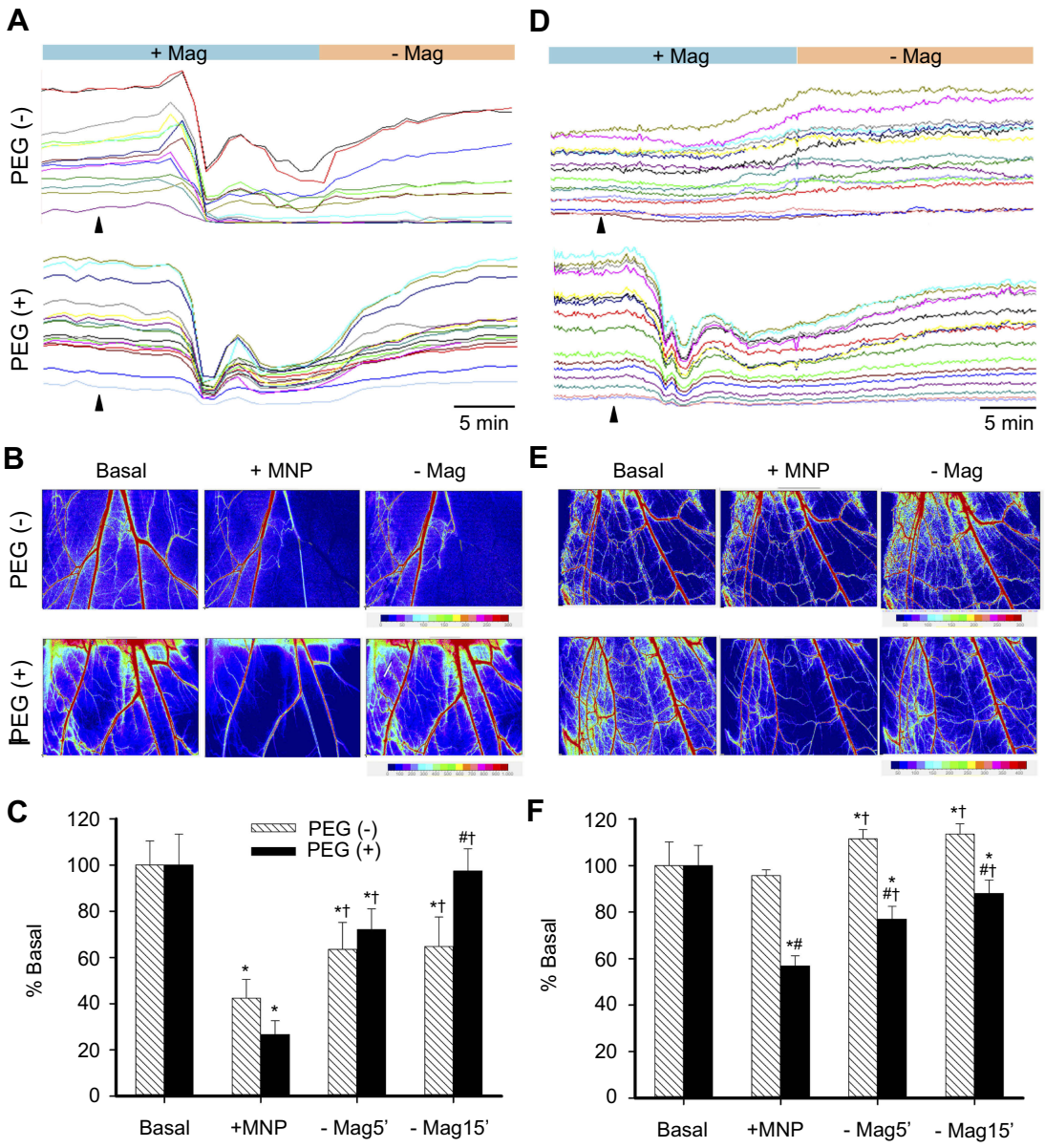

Figure 3 Two-dimensional hemodynamic effects of magnetic capture of PEGylated MNPs in microvessels. RBC flow in cremaster microvessels of individual rats with administration of MNPs of 250- (**A**–**C**) or 50- (**D**–**F**) nm with (+) or without (–) PEG, as indicated, was monitored in a real-time manner. The arrowheads indicate administration of the particles. Speckle images of flow (Flux) with sites of flow acquisition are shown after administration of the particles (**B** and **E**; 5 mg/kg; +MNP) and subsequent magnet removal (-Mag). Effects of PEGylation on magnetic capture of MNPs are summarized (**C** and **F**; n=9–23). $^{*,\#,\dagger}P<0.05$ compared with the corresponding basal, PEG(–) and +MNP groups, respectively.

In contrast, intra-arterial administration of MNPs without PEG caused a gradual increase in the flow of primarily larger vessels under influence of the magnet, with stabilized RBC flow after magnet removal (Figure 3D). Figure 3F illustrates that 4–13 mins after administration of 50 nm MNPs without PEG in magnetic field, the microvascular flow was not altered (n=17 branches from 10 rats), suggesting minimal magnetic capture; whereas PEGylated MNPs of 50 nm significantly reduced basal blood flow by 46% (n=23 branches from 13 rats; $P<0.05$). Fifteen minutes after magnet removal (-Mag), the flow was restored to 87% of basal level in the PEG(+) group.

Figure 4 illustrates representative dynamic retention of PEG(+) MNPs in response to magnetic capture using capillaroscopy. Both gray and color modes of capillaroscopy images display the change in location of MNP agglomerate 12–19 mins after MNP (250 nm) administration with the magnet underneath the cremaster preparation. Even with the magnet in place, the agglomerate of PEG(+)

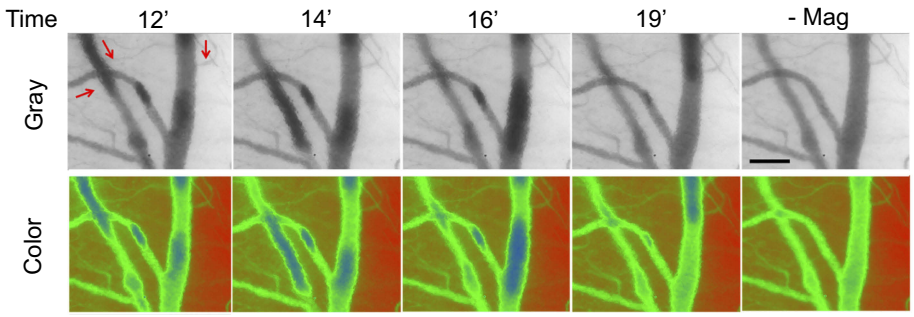

Figure 4 Dynamic retention of MNP with PEG in the representative vessels in magnetic field. Magnetic capture of PEG(+) MNPs (250 nm; 5 mg/kg) in cremaster microcirculation was observed by capillaroscopy under gray and color mode 12–19 mins after administration of the MNPs and 1 min after removal of the magnet (-Mag). The red arrows indicate the flow direction of the adjacent vessel. The results are representative of 6 experiments. Scale bar indicates 50 μm.

MNPs moved along the vessels. After removal of the magnet (-Mag), no retention was observed in any microvessel in this field. In contrast, no such agglomerates were observed after injection of PEG(+) MNPs in the absence of the magnet (Figure S3).

To determine whether PEGylation may exert an effect on magnetic capture of MNPs, MNPs with or without PEG were injected in a silicon tube with serum or hydroxyethyl starch flow at 2 mL/min in circulation, as illustrated in Figure 5A. Magnetic capture of 50 and 250 nm MNPs in hydroxyethyl starch flow was observed 14 sec after co-administration with rat blood in an upstream syringe (Figure 5B). With or without PEGylation, pellet formation occurred in response to the presence of both the magnet and RBC flow; a clear boundary was observed between the pellet and the RBC flow. In experiments without administration of whole blood, MNPs were injected into the flowing serum at 2 mL/min to observe magnetic capture of MNPs without RBC interruption. Pellet formation was observed in the silicon tube by the magnet within 20 sec, followed by gradual reduction of the pellet size in the presence of the magnet and serum flow (Figure 5C). In the 50 nm group, the pellet size of PEG(−) particle was gradually reduced with time and became almost invisible after 480 sec; whereas the pellet size of PEG(+) particles gradually decreased with time, and then increased after 390 sec (Figure 5C). The size of the pellets of 250 nm particles decreased quickly and reached equilibrium between 120 and 600 sec.

The retention areas of 50 and 250 nm particles in Figure 5C are summarized in Figure 5D and E, respectively. At 30 sec, the retention areas of 50 nm particles of PEG(−) and PEG(+) remained at about 72% (Figure 5D), whereas that of 250 nm particles dropped to 36% and 29% (Figure 5E), respectively. However, an increase in the 2-D area of PEG(+) particles was observed after 400 sec, resulting in significantly more particle retention in the group of PEG(+) at the end of observation (Figure 5D; $P<0.05$). In contrast, no significant difference between PEG(−) and PEG(+) groups was observed after 300 sec (Figure 5E).

To determine whether PEGylation may reduce MNP–endothelium interaction and facilitate post-magnet dispersion, 250 nm MNPs with or without PEG were incubated with cultured HUVECs under magnetic field, followed by analysis of cell-associated MNP (MNP_{cell}; Figure 6). Here, the magnet significantly increased MNP_{cell} with and without PEG by 1.3~3.5 and 1.2~3.2 fold, respectively, at 1–6 hrs after administration of MNPs ($P<0.05$). Overall ANOVA indicates a significant difference between the PEG(−) vs (+) groups ($P<0.05$). In the presence of the magnet, PEGylation significantly reduced MNP_{cell} by 46% and 47% at 4 and 6 hrs after administration of MNPs, respectively (n=7, $P<0.05$).

Discussion

Using RBC flow as an indicator, PEGylation has been demonstrated to be able possibly to alter the pattern of dextran-coated MNP retention in response to magnetic capture. To our knowledge, this is the first in vivo demonstration that PEGylated MNPs may be more sensitive to magnetic capture against hemodynamic forces. This was especially prominent for smaller particles, which are associated with an increased hydrodynamic diameter. PEGylation enhanced dispersion of larger magnetite particles after magnet removal, which likely contributed to reduced MNP–MNP and MNP–endothelium interaction.

Our previous studies demonstrated that magnetic capture of PEG(–) MNPs led to visible particle retention in the cremaster vasculature along the magnet margin in the photo view, which was associated with a reduction of tissue perfusion.[11] In this investigation, laser speckle technology with a higher spatial resolution is used, enabling subtle hemodynamic changes that arise from MNP

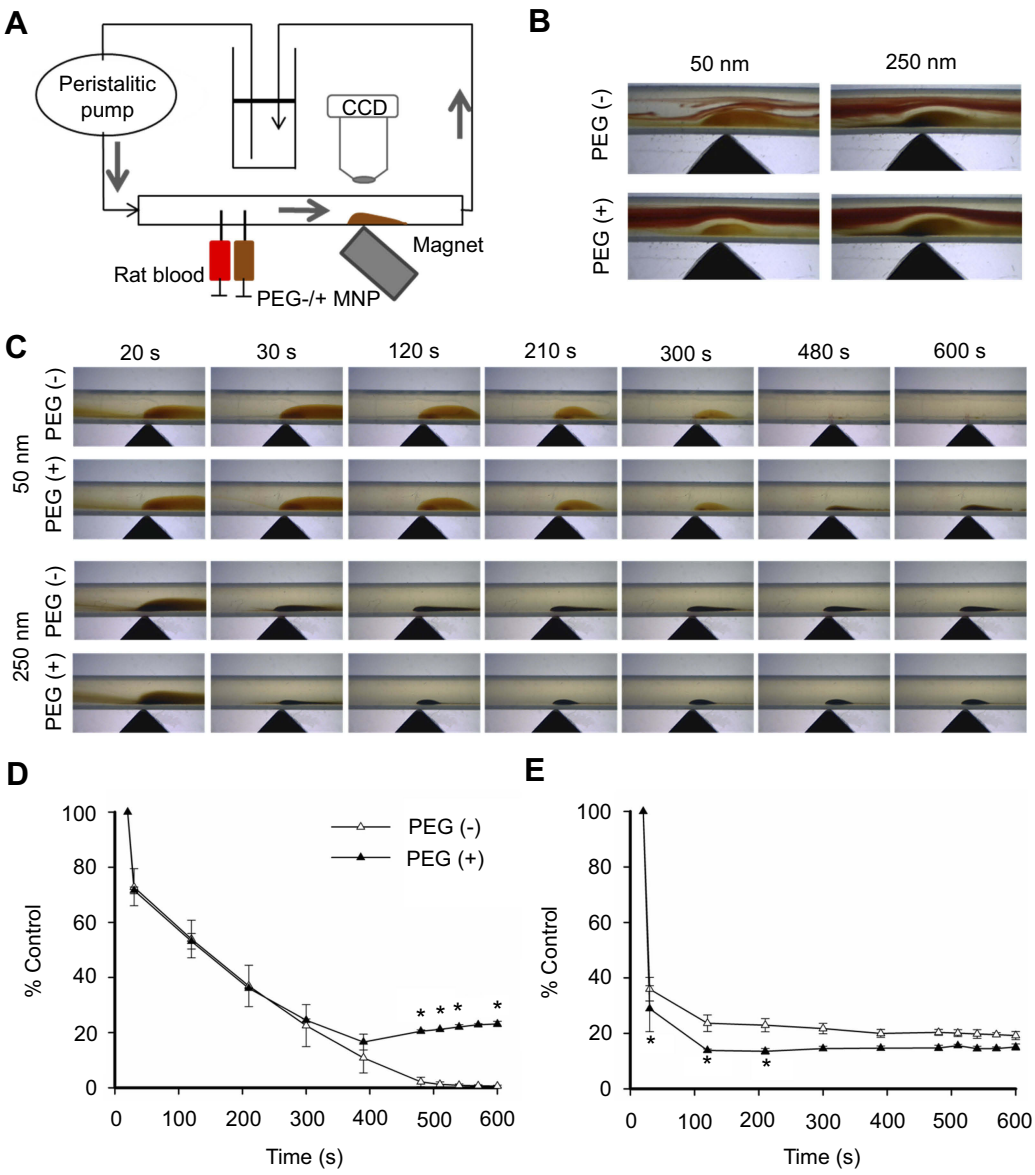

Figure 5 Effects of size and PEGylation on retention of particles subjected to serum/RBC flow and magnetic field. In vitro circulation system (**A**) was established to observe particle retention in hydroxyethyl starch/RBC solution (**B**) or serum (**C**, D, **E**) at 2 mL/min and magnetic field. Summarized 2-D retention of particles of 50 vs 250 nm are presented in (**D**) and (**E**), respectively (n=3). Values are mean ± SEM. *p<0.05 compared with the corresponding PEG(−) groups, respectively.

retention in a single vessel to be recorded. Although significant MNP retention may be observed in a single vessel, blood flow in the microvessel up- and down-stream may still be maintained at a similar level, suggesting that MNP retention does not completely occlude the vessel. Although the structure of PEG may attenuate MNP–endothelium interaction, PEGylation significantly increased the hydrodynamic diameter of especially smaller particles in the serum, which may lead to enhanced magnetic capture.

For the 250 nm nanoparticles, PEGylation facilitates the restoration of tissue flow after magnet removal, which would lessen the potential of any adverse effect on hemodynamics with PEG(+) MNPs in magnetic targeting. PEGylation of MNPs may reduce the packing density of magnetically accumulated MNPs, since the hydrophilic PEG chains would assume an extended conformation in the aqueous phase. This in turn would account for the better dispersibility in circulation,[3,29,49] resulting in dynamic pellet accumulation in magnetic field and fast blood flow restore after magnet removal.

Although no significant changes in averaged RBC flow were observed with 50 nm PEG(–) MNPs in the presence of the magnet, RBC flow in larger vessels gradually increased with time (Figure 3D). It is plausible that the

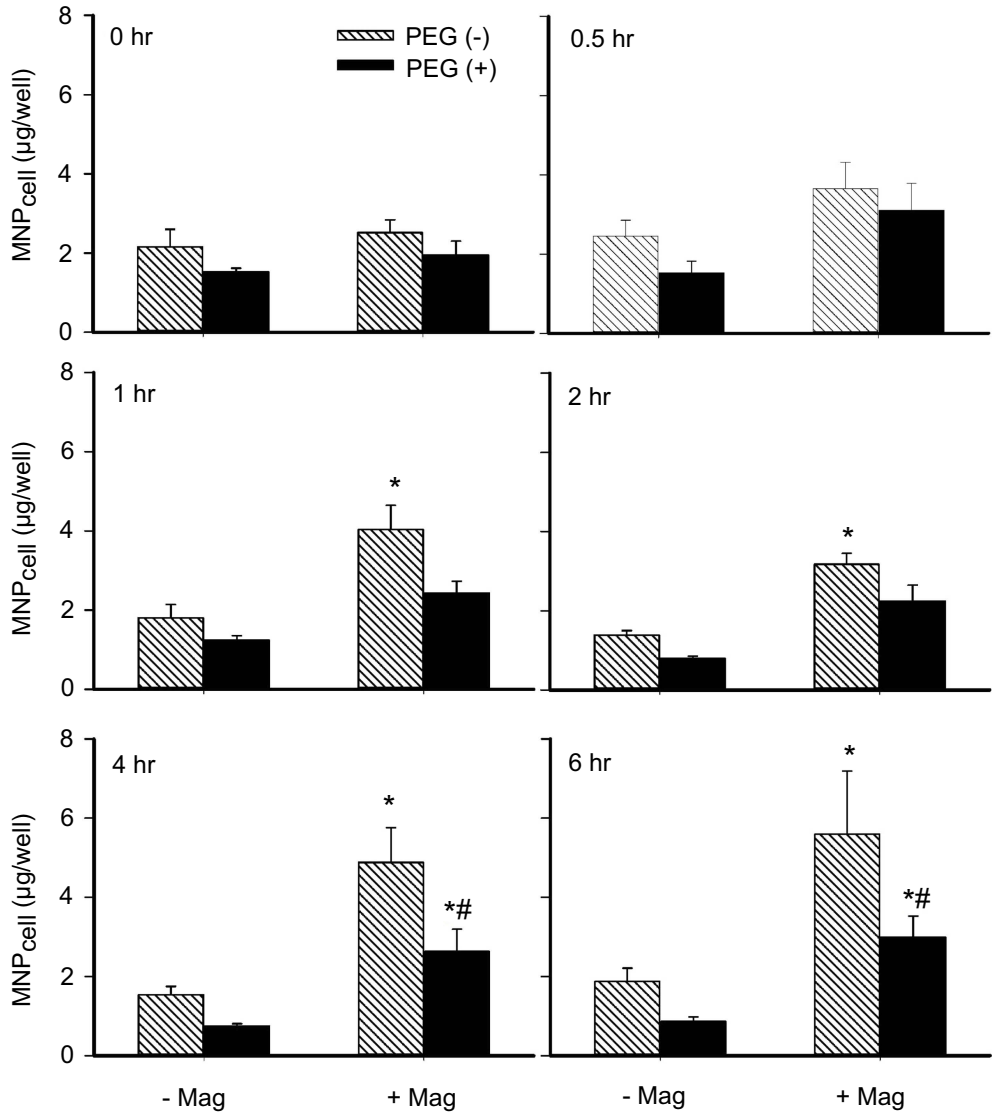

Figure 6 PEGylation attenuated MNP interaction with cultured endothelial cells. Human umbilical vein endothelial cell (HUVEC)-associated MNP was determined after incubation of 250 nm MNP (100 µg/mL; 19.7 µg/cm^2) in the absence (-Mag) and presence (+Mag) of the magnet for up to 6 hrs after application of the magnet for 5 mins to facilitate sedimentation. Values are presented as mean ± SE (n=7). $*^{\#}P<0.05$ compared with the corresponding control (0 hrs) and PEG(−) groups, respectively.

magnetic force acting on the captured PEG(–) MNPs may induce mechanical stimulation upon the endothelium, which is known to release nitric oxide and cause vasodilation.[50] In contrast, PEG may promote agglomeration of smaller MNPs in magnetic field, which reduces RBC flow in microcirculation and facilitates magnetic capture.

In response to magnetic capture in vitro, similar initial particle retention was observed irrespective of particle size and PEGylation in the serum flow (Figure 5C), which allows observation of particle retention with protein corona development. Although the size of the 2-D pellet of the particles may not represent the amount of the particles captured, such a system may provide information concerning particle capture within a short period. Notably, the retention of PEG(+) MNPs of 50 nm gradually declined to only 20%, and thereafter significantly increased, suggesting that the magnet might capture PEG(+) MNPs recirculating to the site of the magnet. In a magnetic field, the capture–escape–recapture cycle probably also occurred in vivo.

Endothelial cells interact with MNPs much less than do tumor cells in culture,[38] possibly favoring the use of MNPs for delivering drugs to treat solid tumors. Although the method employed herein cannot differentiate adsorbed from internalized MNPs, less adhesion is

generally associated with a concomitant less particle internalization.[51] Our results are consistent with previous findings that PEGylated particles exhibit reduced internalization by endothelial cells[38,52] as well as other cells.[37,53] PEGylation may reduce the interaction between the particles and the endothelial cells, which may mediate, at least partially, the altered behavior of PEG(+) MNPs in circulation. The PEGylation-associated dynamic retention of 250 nm particles in response to magnetic force may increase the passage of nanocomposites through the leaky vasculature into the tumor tissue and thereby increase local concentration of the delivered drug.[13,53]

Previous studies have demonstrated a significant difference between the ζ-potential of PEG(−) and PEG(+) MNPs in aqueous solution,[38] distinct behaviors in circulation are not attributed to the ζ-potential of MNPs, probably owing to nearly immediate corona formation after nanoparticles in contact with plasma proteins.[32,54,55] The enhanced capture of smaller PEG(+) MNPs may be attributed to the PEG–plasma protein interaction and then agglomerate formation, resulting in an increased hydrodynamic diameter of MNPs. It has been recently demonstrated that plasma protein adsorption of PEG(+) MNPs, but not bare MNPs, triggers complement activation,[56] which may consequently alter protein corona composition, physical characteristics and particle behaviors in circulation. For larger MNPs, PEGylation may reduce particle–particle interaction induced by magnetic moment generation in magnetic field, and thus enhance MNP escape, allowing dynamic retention of MNPs in vivo. The results herein suggest that PEG(+) MNPs circulation can be magnetically captured. Moreover, the weakening vascular wall–nanoparticle interaction by PEGylation may facilitate blood residence,[27,32] favoring the therapeutic outcome with the target in the circulating blood. Nevertheless, the characteristics of PEGylated nanoparticles may also depend on the composition of the PEG moiety.[45] The molecular weight,[57,58] density[59] and conformation[39,60,61] of PEG may affect nanoparticle–cell interaction,[32,39] the biocompatibility of the nanoparticles,[32,59] and thus their behaviors in circulation. Further studies of the composition of the PEG(+) MNPs coating materials should be undertaken.

Conclusion

This study demonstrates that PEGylation alters the behavior of dextran-coated MNPs in response to magnetic and hemodynamic interaction. In magnetic targeting, the PEG moiety may enhance magnetic capture of PEGylated MNPs and reduce the risk of vessel occlusion by aggregated particles, presumably by attenuating MNP–MNP and MNP–endothelium interaction. Thus, with PEGylated MNPs as drug carriers, therapeutic goals may be potentially achieved in stationary magnetic field. Nevertheless, PEG molecules with different length may form distinct 3-D structure.[32] Whether MNPs with different PEG in length may exert different behavior remains to be determined.

Abbreviation list

APS, ammonium persulfate; DIW, deionized water; ECGS, endothelial cell growth supplement; FBS, fetal bovine serum; HUVEC, human umbilical vein endothelial cells; KSCN, potassium thiocyanate; Mag, magnet; MNPs, magnetic nanoparticles; MNP_{cell}, cell-associated MNP; PBS, phosphate buffered saline; PEG, polyethylene glycol; RBCs, red blood cells; RES, reticuloendothelial system; ROIs, regions of interest.

Acknowledgments

The work was supported by Ministry of Science and Technology (MOST 107-2311-B-182-002-), Chang Gung Memorial Hospital (CMRPD1E0013; BMRP432). Thanks also goes to Timothy Wiedmann, Department of Pharmaceutics, University of Minnesota for editing this manuscript.

Disclosure

The authors report no conflicts of interest in this work.

References

1. Wahajuddin AS. Superparamagnetic iron oxide nanoparticles: magnetic nanoplatforms as drug carriers. *Int J Nanomed*. 2012;7:3445–3471. doi:10.2147/IJN.S30320
2. Reddy LH, Arias JL, Nicolas J, Couvreur P. Magnetic nanoparticles: design and characterization, toxicity and biocompatibility, pharmaceutical and biomedical applications. *Chem Rev*. 2012;112(11):5818–5878. doi:10.1021/cr300068p
3. Singh D, McMillan JM, Liu XM, et al. Formulation design facilitates magnetic nanoparticle delivery to diseased cells and tissues. *Nanomedicine*. 2014;9(3):469–485. doi:10.2217/nnm.14.4
4. Shen L, Li B, Qiao Y. Fe_3O_4 nanoparticles in targeted drug/gene delivery systems. *Materials*. 2018;11(2):324. doi:10.3390/ma11081451
5. Ulbrich K, Holá K, Šubr V, Bakandritsos A, Tuček J, Zbořil R. Targeted drug delivery with polymers and magnetic nanoparticles: covalent and noncovalent approaches, release control, and clinical studies. *Chem Rev*. 2016;116(9):5338–5431. doi:10.1021/acs.chemrev.5b00589
6. Mody VV, Cox A, Shah S, Singh A, Bevins W, Parihar H. Magnetic nanoparticle drug delivery systems for targeting tumor. *Appl Nanosci*. 2013;4(4):385–392. doi:10.1007/s13204-013-0216-y
7. Amstad E, Textor M, Reimhult E. Stabilization and functionalization of iron oxide nanoparticles for biomedical applications. *Nanoscale*. 2011;3(7):2819–2843. doi:10.1039/c1nr10173k

8. Janikowska A, Matuszak J, Lyer S, et al. A novel human artery model to assess the magnetic accumulation of SPIONs under flow conditions. *Sci Rep*. 2017;7:42314. doi:10.1038/srep42314
9. Zhao Q, Wang L, Cheng R, et al. Magnetic nanoparticle-based hyperthermia for head & neck cancer in mouse models. *Theranostics*. 2012;2(1):113–121. doi:10.7150/thno.3854
10. Liu HL, Hua MY, Yang HW, et al. Magnetic resonance monitoring of focused ultrasound/magnetic nanoparticle targeting delivery of therapeutic agents to the brain. *Proc Natl Acad Sci U S A*. 2010;107 (34):15205–15210. doi:10.1073/pnas.1003388107
11. Ma YH, Chen SY, Tu SJ, Yang HW, Liu HL. Manipulation of magnetic nanoparticle retention and hemodynamic consequences in microcirculation: assessment by laser speckle imaging. *Int J Nanomed*. 2012;7:2817–2827. doi:10.2147/IJN.S31730
12. Tu SJ, Wu SY, Wang FS, Ma YH. Retention assessment of magnetic nanoparticles in rat arteries with micro-computed tomography. *Phys Med Biol*. 2014;59(5):1271–1281. doi:10.1088/0031-9155/59/5/1271
13. Yang HW, Hua MY, Hwang TL, et al. Non-invasive synergistic treatment of brain tumors by targeted chemotherapeutic delivery and amplified focused ultrasound-hyperthermia using magnetic nanographene oxide. *Adv Mater*. 2013;25(26):3605–3611. doi:10.1002/adma.201301046
14. Shen JM, Guan XM, Liu XY, Lan JF, Cheng T, Zhang HX. Luminescent/magnetic hybrid nanoparticles with folate-conjugated peptide composites for tumor-targeted drug delivery. *Bioconj Chem*. 2012;23(5):1010–1021. doi:10.1021/bc300008k
15. Ma YH, Hsu YW, Chang YJ, Hua MY, Chen JP, Wu T. Intra-arterial application of magnetic nanoparticles for targeted thrombolytic therapy: a rat embolic model. *J Magn Magn Mater*. 2007;311 (1):342–346. doi:10.1016/j.jmmm.2006.10.1204
16. Schleich N, Po C, Jacobs D, et al. Comparison of active, passive and magnetic targeting to tumors of multifunctional paclitaxel/SPIO-loaded nanoparticles for tumor imaging and therapy. *J Control Release*. 2014;194:82–91. doi:10.1016/j.jconrel.2014.07.059
17. Ma YH, Wu SY, Wu T, Chang YJ, Hua MY, Chen JP. Magnetically targeted thrombolysis with recombinant tissue plasminogen activator bound to polyacrylic acid-coated nanoparticles. *Biomaterials*. 2009;30(19):3343–3351. doi:10.1016/j.biomaterials.2009.02.034
18. Yang HW, Hua MY, Lin KJ, et al. Bioconjugation of recombinant tissue plasminogen activator to magnetic nanocarriers for targeted thrombolysis. *Int J Nanomed*. 2012;7:5159–5173.
19. Tadayon A, Jamshidi R, Esmaeili A. Targeted thrombolysis of tissue plasminogen activator and streptokinase with extracellular biosynthesis nanoparticles using optimized Streptococcus equi supernatant. *Int J Pharm*. 2016;501(1–2):300–310. doi:10.1016/j.ijpharm.2016.02.011
20. Che E, Gao Y, Wan L, et al. Paclitaxel/gelatin coated magnetic mesoporous silica nanoparticles: preparation and antitumor efficacy in vivo. *Microporous Mesoporous Mat*. 2015;204:226–234. doi:10.1016/j.micromeso.2014.11.013
21. Bai J, Wang JTW, Rubio N, et al. Triple-modal imaging of magnetically-targeted nanocapsules in solid tumours *in vivo*. *Theranostics*. 2016;6(3):342–356. doi:10.7150/thno.11918
22. Cui Y, Zhang M, Zeng F, Jin H, Xu Q, Huang Y. Dual-targeting magnetic PLGA nanoparticles for codelivery of paclitaxel and curcumin for brain tumor therapy. *ACS Appl Mater Interfaces*. 2016;8 (47):32159–32169. doi:10.1021/acsami.6b10175
23. Liao J, Wei X, Ran B, Peng J, Qu Y, Qian Z. Polymer hybrid magnetic nanocapsules encapsulating IR820 and PTX for external magnetic field-guided tumor targeting and multifunctional theranostics. *Nanoscale*. 2017;9(7):2479–2491. doi:10.1039/c7nr00033b
24. Varna M, Juenet M, Bayles R, Mazighi M, Chauvierre C, Letourneur D. Nanomedicine as a strategy to fight thrombotic diseases. *Future Sci OA*. 2015;1(4). doi:10.4155/fso.15.46
25. Chen JP, Liu CH, Hsu HL, Wu T, Lu YJ, Ma YH. Magnetically controlled release of recombinant tissue plasminogen activator from chitosan nanocomposites for targeted thrombolysis. *J Mater Chem B*. 2016;4(15):2578–2590. doi:10.1039/C5TB02579F
26. Petros RA, DeSimone JM. Strategies in the design of nanoparticles for therapeutic applications. *Nat Rev Drug Discov*. 2010;9 (8):615–627. doi:10.1038/nrd2591
27. Elsabahy M, Wooley KL. Design of polymeric nanoparticles for biomedical delivery applications. *Chem Soc Rev*. 2012;41 (7):2545–2561. doi:10.1039/c2cs15327k
28. Abboud M, Youssef S, Podlecki J, Habchi R, Germanos G, Foucaran A. Superparamagnetic Fe_3O_4 nanoparticles, synthesis and surface modification. *Mater Sci Semicond Process*. 2015;39:641–648. doi:10.1016/j.mssp.2015.05.035
29. Kolate A, Baradia D, Patil S, Vhora I, Kore G, Misra A. PEG – a versatile conjugating ligand for drugs and drug delivery systems. *J Control Release*. 2014;192:67–81. doi:10.1016/j.jconrel.2014.06.046
30. Rabanel JM, Hildgen P, Banquy X. Assessment of PEG on polymeric particles surface, a key step in drug carrier translation. *J Control Release*. 2014;185:71–87. doi:10.1016/j.jconrel.2014.04.017
31. Gref R, Domb A, Quellec P, et al. The controlled intravenous delivery of drugs using PEG-coated sterically stabilized nanospheres. *Adv Drug Del Rev*. 2012;64(Supplement):316–326. doi:10.1016/j.addr.2012.09.008
32. Pelaz B, Del Pino P, Maffre P, et al. Surface functionalization of nanoparticles with polyethylene glycol: effects on protein adsorption and cellular uptake. *ACS Nano*. 2015;9(7):6996–7008. doi:10.1021/acsnano.5b01326
33. Oberoi HS, Nukolova NV, Kabanov AV, Bronich TK. Nanocarriers for delivery of platinum anticancer drugs. *Adv Drug Del Rev*. 2013;65 (13–14):1667–1685. doi:10.1016/j.addr.2013.09.014
34. Fang RH, Hu CM, Zhang L. Nanoparticles disguised as red blood cells to evade the immune system. *Expert Opin Biol Ther*. 2012;12 (4):385–389. doi:10.1517/14712598.2012.661710
35. Lim EK, Jang E, Lee K, Haam S, Huh YM. Delivery of cancer therapeutics using nanotechnology. *Pharmaceutics*. 2013;5(2):294. doi:10.3390/pharmaceutics5020294
36. Hu FQ, Zhang YY, You J, Yuan H, Du YZ. pH triggered doxorubicin delivery of PEGylated glycolipid conjugate micelles for tumor targeting therapy. *Mol Pharm*. 2012;9(9):2469–2478. doi:10.1021/mp300002v
37. Qu JB, Shao HH, Jing GL, Huang F. PEG-chitosan-coated iron oxide nanoparticles with high saturated magnetization as carriers of 10-hydroxycamptothecin: preparation, characterization and cytotoxicity studies. *Colloid Surf B-Biointerfaces*. 2013;102:37–44. doi:10.1016/j.colsurfb.2012.08.004
38. Lu YC, Luo PC, Huang CW, et al. Augmented cellular uptake of nanoparticles using tea catechins: effect of surface modification on nanoparticle-cell interaction. *Nanoscale*. 2014;6(17):10297–10306. doi:10.1039/c4nr00617h
39. Onyskiw PJ, Eniola-Adefeso O. Effect of PEGylation on ligand-based targeting of drug carriers to the vascular wall in blood flow. *Langmuir*. 2013;29(35):11127–11134. doi:10.1021/la402182j
40. Siow WX, Chang YT, Babic M, Lu YC, Horak D, Ma YH. Interaction of poly-l-lysine coating and heparan sulfate proteoglycan on magnetic nanoparticle uptake by tumor cells. *Int J Nanomed*. 2018;13:1693–1706. doi:10.2147/IJN.S156029
41. Matuszak J, Zaloga J, Friedrich RP, et al. Endothelial biocompatibility and accumulation of SPION under flow conditions. *J Magn Magn Mater*. 2015;380:20–26. doi:10.1016/j.jmmm.2014.09.005
42. Friedrich RP, Janko C, Poettler M, et al. Flow cytometry for intracellular SPION quantification: specificity and sensitivity in comparison with spectroscopic methods. *Int J Nanomed*. 2015;10:4185–4201. doi:10.2147/IJN.S82714
43. Lu Q, Ye F, Yang X, et al. Accelerated recovery of endothelium function after stent implantation with the use of a novel systemic nanoparticle curcumin. *Biomed Res Int*. 2015;2015(2015):291871. doi:10.1155/2015/291871
44. Zapotoczny S, Szczubialka K, Nowakowska M. Nanoparticles in endothelial theranostics. *Pharmacol Rep*. 2015;67(4):751–755. doi:10.1016/j.pharep.2015.05.018

45. Silvestri A, Di Silvio D, Llarena I, et al. Influence of surface coating on the intracellular behaviour of gold nanoparticles: a fluorescence correlation spectroscopy study. *Nanoscale*. 2017;9(38):14730–14739. doi:10.1039/c7nr04640e
46. Lin YL, Lin YC, Wang LJ, Ngo ST, Ma YH. Renal perfusion assessment using magnetic nanoparticles with 7T dynamic susceptibility contrast MRI in rats. *J Magn Magn Mater*. 2019;475:76–82. doi:10.1016/j.jmmm.2018.11.041
47. Gultepe E, Reynoso FJ, Jhaveri A, et al. Monitoring of magnetic targeting to tumor vasculature through MRI and biodistribution. *Nanomedicine (Lond)*. 2010;5(8):1173–1182. doi:10.2217/nnm.10.84
48. Windberger U, Bartholovitsch A, Plasenzotti R, Korak KJ, Heinze G. Whole blood viscosity, plasma viscosity and erythrocyte aggregation in nine mammalian species: reference values and comparison of data. *Exp Physiol*. 2003;88(3):431–440.
49. Bunker A. Poly(ethylene glycol) in drug delivery, why does it work, and can we do better? All atom molecular dynamics simulation provides some answers. *Phys Procedia*. 2012;34:24–33. doi:10.1016/j.phpro.2012.05.004
50. Erkens R, Suvorava T, Kramer CM, Diederich LD, Kelm M, Cortese-Krott MM. Modulation of local and systemic heterocellular communication by mechanical forces: a role of endothelial nitric oxide synthase. *Antioxid Redox Signal*. 2017;26(16):917–935. doi:10.1089/ars.2016.6904
51. Lesniak A, Salvati A, Santos-Martinez MJ, Radomski MW, Dawson KA, Aberg C. Nanoparticle adhesion to the cell membrane and its effect on nanoparticle uptake efficiency. *J Am Chem Soc*. 2013;135(4):1438–1444. doi:10.1021/ja309812z
52. Yu M, Huang S, Yu KJ, Clyne AM. Dextran and polymer polyethylene glycol (PEG) coating reduce both 5 and 30 nm iron oxide nanoparticle cytotoxicity in 2D and 3D cell culture. *Int J Mol Sci*. 2012;13(5):5554. doi:10.3390/ijms13055554
53. Yang HW, Hua MY, Liu HL, et al. Self-protecting core-shell magnetic nanoparticles for targeted, traceable, long half-life delivery of BCNU to gliomas. *Biomaterials*. 2011;32(27):6523–6532. doi:10.1016/j.biomaterials.2011.05.047
54. Fleischer CC, Payne CK. Nanoparticle-cell interactions: molecular structure of the protein corona and cellular outcomes. *Accounts Chem Res*. 2014;47(8):2651–2659. doi:10.1021/ar500190q
55. Sakulkhu U, Mahmoudi M, Maurizi L, Salaklang J, Hofmann H. Protein corona composition of superparamagnetic iron oxide nanoparticles with various physico-chemical properties and coatings. *Sci Rep*. 2014;4:5020. doi:10.1038/srep05020
56. Escamilla-Rivera V, Solorio-Rodríguez A, Uribe-Ramírez M, et al. Plasma protein adsorption on Fe(3)O(4)-PEG nanoparticles activates the complement system and induces an inflammatory response. *Int J Nanomed*. 2019;14:2055–2067. doi:10.2147/IJN.S192214
57. Rahme K, Chen L, Hobbs RG, Morris MA, O'Driscoll C, Holmes JD. PEGylated gold nanoparticles: polymer quantification as a function of PEG lengths and nanoparticle dimensions. *RSC Adv*. 2013;3(17):6085–6094.
58. Riedinger A, Guardia P, Curcio A, et al. Subnanometer local temperature probing and remotely controlled drug release based on azo-functionalized iron oxide nanoparticles. *Nano Lett*. 2013;13(6):2399–2406. doi:10.1021/nl400188q
59. Xu Q, Ensign LM, Boylan NJ, et al. Impact of surface polyethylene glycol (PEG) density on biodegradable nanoparticle transport in mucus ex vivo and distribution in vivo. *ACS Nano*. 2015;9(9):9217–9227. doi:10.1021/acsnano.5b03876
60. Li J, Sharkey CC, Huang D, King MR. Nanobiotechnology for the therapeutic targeting of cancer cells in blood. *Cell Mol Bioeng*. 2015;8(1):137–150. doi:10.1007/s12195-015-0381-z
61. Decuzzi P, Godin B, Tanaka T, et al. Size and shape effects in the biodistribution of intravascularly injected particles. *J Control Release*. 2010;141(3):320–327. doi:10.1016/j.jconrel.2009.10.014

Supplementary material

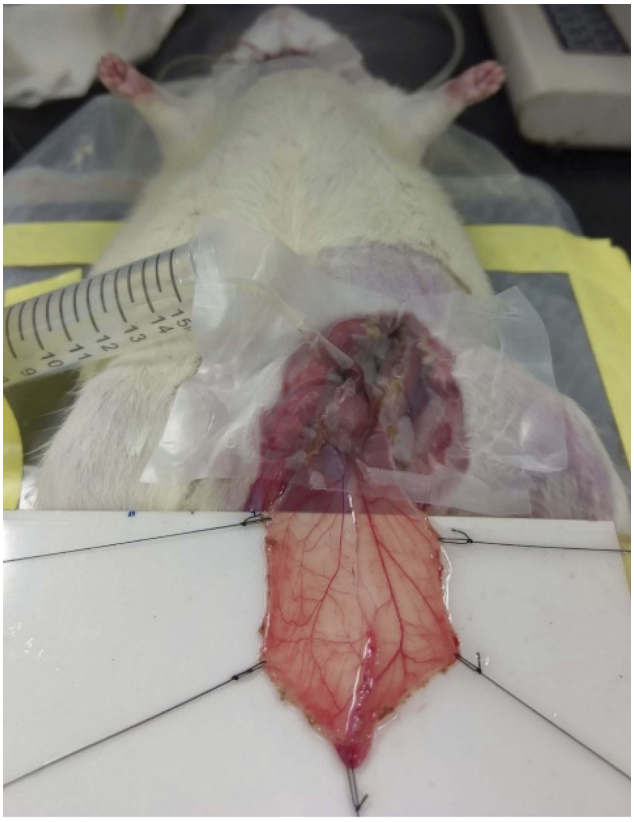

Figure S1 Cremaster muscle preparation of an anesthetized rat. Left cremaster muscle was spread with tension created by suture on a home-made platform. The muscle preparation was then subjected to laser speckle contrast imaging or cappillaroscipy from above.

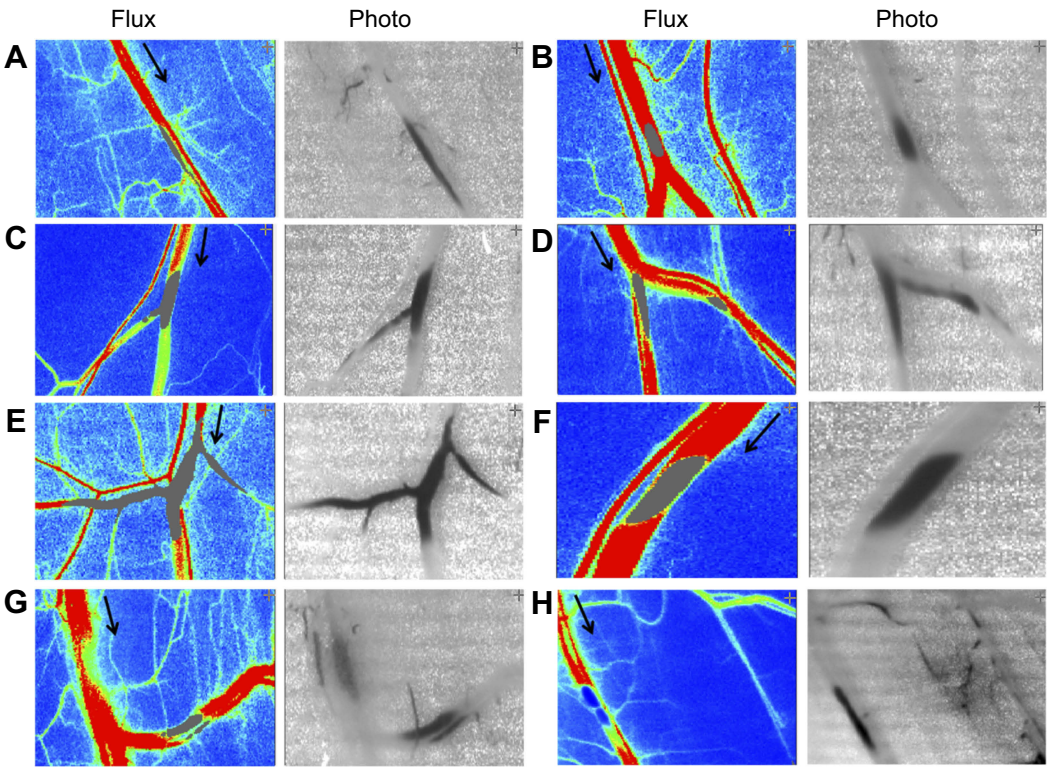

Figure S2 Magnetic capture of MNP and subsequent flow changes in microvessels. MNPs (5 mg/kg) were administered intra-arterially to the left cremaster muscle with a NdFeB magnet placed underneath. MNP accumulation 1 to 14 mins after administration is illustrated as flux and photo images. The arrow in the flux images indicates the flow direction of the adjacent vessel. Patterns of magnetic capture of MNPs in microvessels (**A**–**H**) were observed.

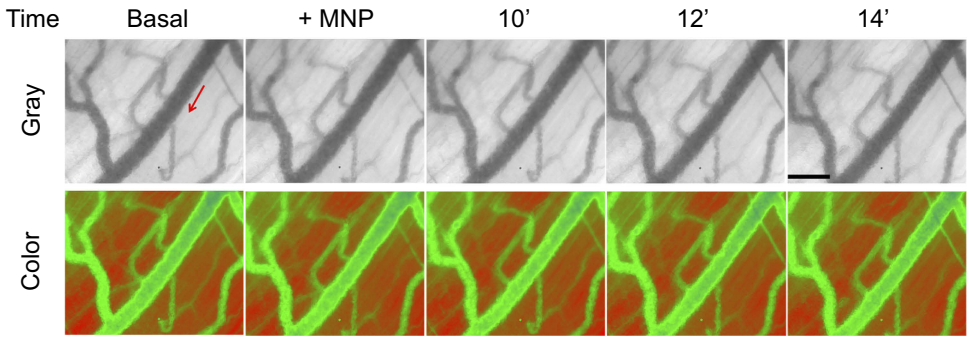

Figure S3 Dynamic retention of MNP with PEG in the representative vessels without magnetic field. Without magnetic capture of PEGylated MNPs (250 nm; 5 mg/kg) in cremaster microcirculation was observed by capillaroscopy under gray and color mode 12–19 mins after administration of the MNPs. The red arrows indicate the flow direction of the adjacent vessel. The results are representative of 6 experiments. Scale bar indicates 50 μm.